J. Fluid Mech. (2002), *vol.* 460, *pp.* 223–240. © 2002 Cambridge University Press
DOI: 10.1017/S0022112002008182 Printed in the United Kingdom

Eigenmode resonance in a two-layer stratification

By ISAO KANDA AND P. F. LINDEN

Department of Mechanical and Aerospace Engineering, University of California, San Diego, La Jolla, CA 92093-0411, USA

(Received 21 March 2001 and in revised form 21 November 2001)

In this paper, we study the velocity field at the density interface of a two-layer stratification system when the flow is forced at the mid-depth of the lower layer by the source–sink forcing method. It is known that, in a sufficiently strong linear stratification, the source–sink forcing in certain configurations produces a single-vortex pattern which corresponds to the lowest eigenmode of the Helmholtz equation (Kanda & Linden 2001). Two types of forcing configuration are used for the two-layer experiments: one that leads to a steady single-vortex pattern in a linear stratification, and one that results in an unsteady irregular state. Strong single-vortex patterns appear intermittently for the former configurations despite the absence of stratification at the forcing height. When the single-vortex pattern occurs at the density interface, a similar flow field extends down to the forcing height. The behaviour is explained as the coupling of the resonant eigenmode at the interface with the horizontal component of the forcing jets. The results show that stratification can organise a flow, even though it is forced by an apparently random three-dimensional forcing.

1. Introduction

In our previous paper (Kanda & Linden 2001, hereinafter referred to as KL), we studied the interaction of multiple laminar jets in a linear stratification. The jets are at the same vertical height and are issued from the boundary walls of a square domain. Among various horizontal velocity fields, we found steady flow patterns which do not reflect the symmetry of the jet configuration. They were explained as resonant eigenmodes of the Helmholtz equation for the streamfunction. The explanation, however, involved an assumption that the Helmholtz equation is chosen out of all possible solutions to the vorticity equation. The assumption was not justified in mechanical terms, but was supported by the fact that the observed relations between the streamfunction and the vorticity are approximately the same as those of the eigenmodes of the Helmholtz equation. Eigenmode resonance is necessary for the observed steady states to appear, but our observations were limited to the final results of resonance and we did not show the transient stage toward resonance. In this paper, by using a two-layer stratification, we present the transient stage and provide further support for our assumptions. We also obtain preliminary results on the relation between the forcing configurations and the resulting velocity field. Two-layer stratification has analogues in oceanic thermoclines, the upper troposphere, and many industrial situations, and our results provide a new perspective on the horizontal structures and mixing in such fluids.

First, we summarize our previous paper in more detail. In a linear stratification, laminar horizontal jets are introduced by source–sink forcing. The source–sink method, originally used by Boubnov, Dalziel & Linden (1994), employs injection and suction

https://doi.org/10.1017/S0022112002008182 Published online by Cambridge University Press

pipes on the domain sidewalls, and ensures mass conservation and unrestricted interaction of jets inside the domain. With four source–sink forcing pairs, we found that some of the steady states have streamlines similar to eigenmodes of the Helmholtz equation. A steady state can be approximated as an inviscid two-dimensional flow and the Helmholtz equation for the streamfunction is one possible solution to the vorticity equation. When the forcing geometry is perfectly symmetric and does not impart any net angular momentum, a solution to the Helmholtz equation has the same symmetry as the forcing geometry and the observed eigenmode structures with significant circulation do not appear. However, small deviations from perfect symmetry allow such eigenmode structures. An eigenmode attains a dominant amplitude when the proportionality constant between the vorticity and the streamfunction is close to the corresponding eigenvalue for the given domain; otherwise the eigenmode has small amplitude in proportion to the deviations. This resonant amplification is the result of unintended net angular momentum. For three different steady states, we obtained good agreement between the analytical solutions and the observations. Although the eigenmode argument applies to any forcing configuration, the resonant behaviour is observed only for certain configurations and we do not know the relation between the forcing configurations and the resultant flows. The eigenmode argument was introduced to explain the appearance of some steady states with significant circulation. The relation between the forcing configurations and the resulting flows should be investigated by taking account of the dynamics of individual forcing jets.

In this paper, we use a two-layer stratification which reveals the transient stage of the resonant behaviour. The source–sink forcing pipes are placed at the mid-depth of the lower layer. The source jets interact three-dimensionally in the homogeneous fluid and induce horizontal flows at the density interface. Due to additional freedom of motion, this setup reduces the probability of eigenmode resonance and makes the resonant state less stable to disturbances. Two types of forcing configurations are tested: one that results in a single-vortex pattern (the lowest eigenmode) in a linear stratification, and another that results in unsteady irregular states in a linear stratification. For the former type of configuration which introduces less disturbances, we observe recurrence of the resonant state with distinctly larger kinetic energy than non-resonant states.

The outline of this paper is as follows. In § 2 we describe the apparatus and the procedure of the two-layer experiments. We derive an empirical rule of pattern formation in a linear stratification and select forcing configurations to be used in the two-layer experiments. In § 3 we show the results of long-term observations and identify resonant amplification of the lowest eigenmode. In § 4 we discuss the implications and applications of the results.

2. Experimental method

2.1. *Apparatus*

The apparatus shown in figure 1 is the same as the one used in KL. The inner dimension of the tank is $59.7 \times 59.7 \times 40.6$ cm. Salt water of density $1.036\,\mathrm{g\,cm^{-3}}$ is filled up to 20 cm. Kerosine (density $0.80\,\mathrm{g\,cm^{-3}}$) is poured on top of the salt water until it forms a 1.1 cm layer. Kerosine is immiscible with salt water and a sharp density interface is maintained. The relatively thin kerosine layer allows fast establishment of horizontal two-dimensional motion in the layer. Four, eight, or twelve source–sink forcing pairs are set on the sidewalls at the mid-depth of the salt water layer. The

https://doi.org/10.1017/S0022112002008182 Published online by Cambridge University Press

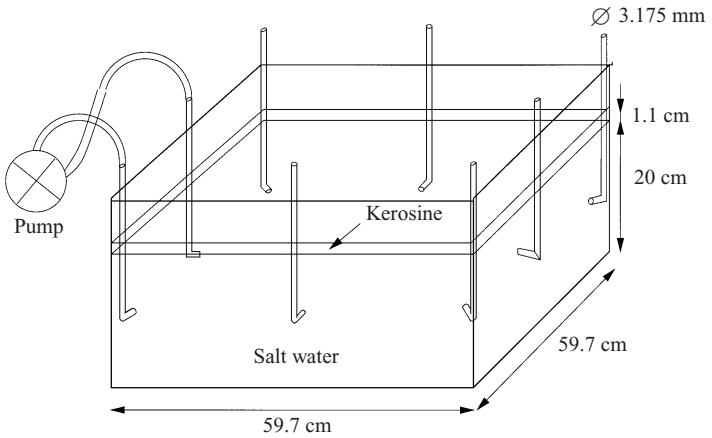


FIGURE 1. Apparatus showing a four-pair configuration. All the forcing pipes are connected to the channels of a peristaltic pump.

sources and sinks are made of 3.175 mm inner diameter pipes bent at a right angle near the orifices. They are connected to individual channels of a peristaltic pump and the fluid sucked into the sinks is re-introduced from the sources. The source–sink pairs are placed in configurations such that they do not impart any significant net thrust or net angular momentum. In the next subsection, we choose forcing configurations according to the resultant velocity field in a linear stratification. The mean velocity V at the orifices of each source–sink pair is fixed at $2.3\,\mathrm{cm\,s^{-1}}$ with variation among the pairs at most 10%. The Reynolds number Vd/ν, where d is the orifice diameter and ν is the kinematic viscosity of salt water, is thus 730. Each source produces a horizontal jet and each sink produces a velocity field similar to half the potential field of a point sink. In a linear stratification, Boubnov *et al.* (1994) show that the source jets cause mixing and the velocity field becomes three-dimensional in buoyancy time 10^5 if the Froude number V/Nd, where N is the buoyancy frequency of the initial stratification, is larger than 15. In the bulk of the homogeneous salt water layer, the Froude number is infinite and the source jets immediately interact three-dimensionally. At the density interface, horizontal flow is induced by this irregular flow. For flow visualization, Pliolite VT particles (Goodyear chemicals, mean density $\sim 1.022\,\mathrm{g\,cm^{-3}}$, size $850 \sim 1180\,\mu\mathrm{m}\,\phi$) are seeded at the density interface. Since the particles are polymers and dissolve in kerosine in about an hour, they have to be replenished on each observation occasion. The particles are illuminated by horizontal slit light and the motion is recorded through a CCD camera from above. The velocity field is analysed by DigImage, a particle tracking system developed at DAMTP, Cambridge (Dalziel 1993).

Each experiment runs for three days with daytime observation at 1 to 3 h intervals. No observation is done at night. At the end of the third day, the reaction product of kerosine and Pliolite forms a thin white layer at the interface, and the resulting weak intensity contrast of the recorded images makes particle tracking difficult. However, no monotonic deceleration of the interfacial motion is observed due to this white layer. Because we seed a small number of particles to ensure long-term observation without thickening of the white layer and also because chemical reaction causes fading or coagulation of particles, the analysed velocity data are missing or spurious at some grid points. Spurious velocity data often have singularly large magnitudes

https://doi.org/10.1017/S0022112002008182 Published online by Cambridge University Press

and are manually removed before calculating the average velocity magnitude of the domain. The essential features are not affected by this rough analysis.

2.2. *Forcing configurations*

Forcing configurations are chosen according to the resultant velocity field in a linear stratification. A linear stratification of salt water is established by the double-bucket method. The depth of the fluid is 20 cm and the constant buoyancy frequency is $1.5\,\mathrm{s}^{-1}$. The Pliolite VT particles are seeded at about 13 cm from the bottom of the tank and the source–sink forcing pairs are set at the level of the seeded layer. The source flow rate is $2.3\,\mathrm{cm\,s}^{-1}$ and the induced flow is horizontal and laminarized as shown in figure 2 of KL.

We select two types of forcing configurations: one that results in the stable single-vortex pattern and another that results in an unsteady irregular velocity field. Although we found three different eigenmode structures for four-pair forcing in KL, the single-vortex pattern (the lowest eigenmode) is the only steady state common in various source–sink forcing experiments: eight pairs in a square domain in KL and Boubnov *et al.* (1994), and twenty and forty pairs in a circular domain in Linden, Boubnov & Dalziel (1995). Unsteady irregular states were first found by KL for four- and eight-pair configurations. Until then it was believed that, if the induced flow is sufficiently horizontal and laminarized, the flow eventually evolves into a single dominant vortex through merger of like-sign vortices and shearing-out of weak vortices irrespective of the forcing configuration. Boubnov *et al.* (1994) show temporal evolution from an unsteady irregular state to the steady single-vortex pattern for their fixed eight-pair forcing configuration. The time necessary to reach the single-vortex pattern depends on the Froude number V/Nd. KL's finding is that the formation of the single-vortex pattern is very sensitive to the forcing configuration; some configurations immediately result in the single-vortex pattern, but others never reach a steady state. Here we seek configurations which result in either of these states.

Previous experiments show that the single-vortex pattern appears quickly when the source jets are directed toward the centre of the domain. This conforms to a qualitative picture where multiple jets meeting at the central point deflect each other clockwise or counterclockwise and finally evolve into a single vortex occupying the domain. We expect that the unsteady irregular state results when the colliding points of the source jets are distributed in the domain.

The experimental results for four, eight, and twelve source–sink pairs in a linear stratification are shown in figure 2. The four-pair case is thoroughly studied in KL. The single-vortex pattern always appears when the source jets are placed at the corners and directed toward the centre (figure 2*a*). Putting the source jets at one-third points on the sidewalls makes the jets collide at two separate points in the domain, but this configuration is known to result in a steady four-vortex pattern. However, by putting the source jets at the mid-points of the sidewalls and directing them toward the centre, a five-vortex instead of the single-vortex pattern appears in one out of five trials, and an unsteady irregular state develops in other trials (figure 2*d*). Hence we choose this configuration as the one leading to the unsteady irregular state. For the eight-pair case, the single-vortex pattern always appears when the source jets are placed at the corners and the mid-points of the sidewalls, and are directed toward the centre (figure 2*b*). When the sources and sinks are exchanged, an unsteady irregular state always results (figure 2*e*). For the twelve-pair case, the single-vortex pattern always appears when the source jets are at the corners and at one-third and two-third points on the sidewalls, and are directed toward the centre (figure 2*c*). If the source

https://doi.org/10.1017/S0022112002008182 Published online by Cambridge University Press

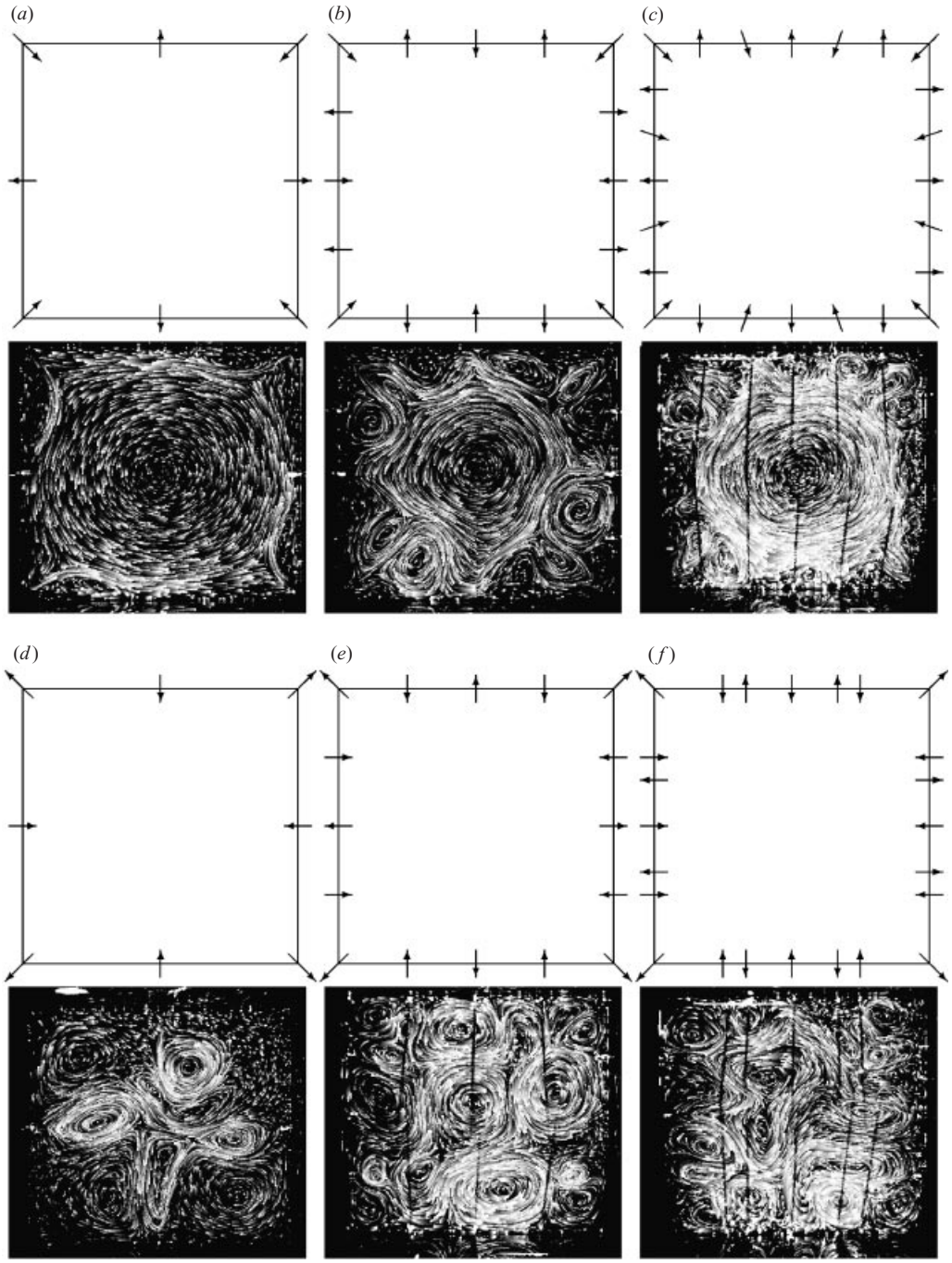


FIGURE 2. Streak images of forcing experiments in a linear stratification. (*a–c*) Configurations resulting in a dominant single vortex as a steady state. (*d–f*) Configurations resulting in an irregular unsteady state. Arrows denote sources and sinks.

jets on the sidewalls are directed perpendicular to the sidewalls, the central vortex deforms significantly (figure 3*a*). When the source jets are placed at one-quarter, one-half, and three-quarter points of the sidewalls, the velocity field is unsteady and irregular (figure 2*f*). If the source jets are placed at one-sixth, one-half, and five-sixth

https://doi.org/10.1017/S0022112002008182 Published online by Cambridge University Press

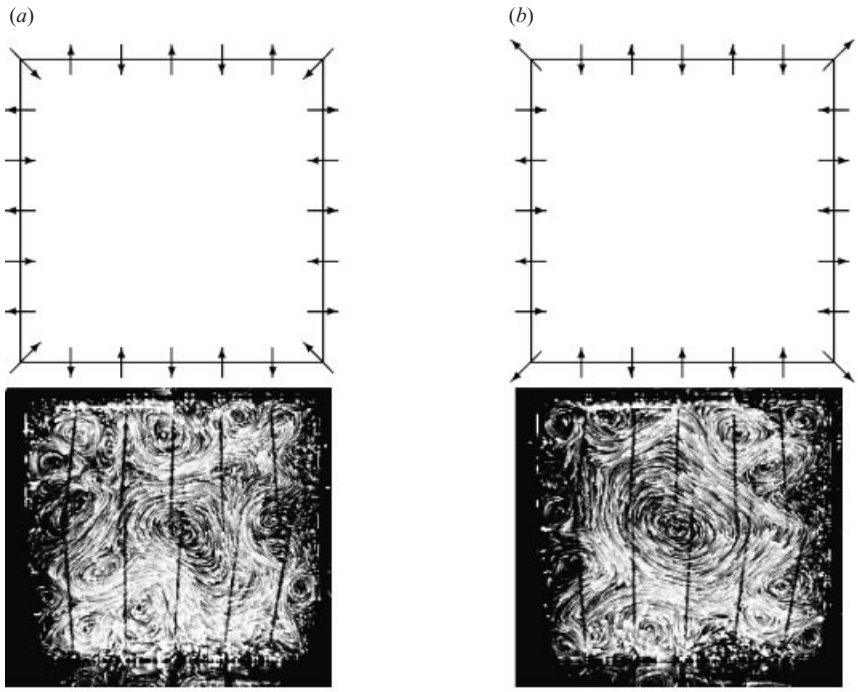


FIGURE 3. Twelve-pair forcing in a linear stratification. (*a*) Source jets on the sidewalls are not directed toward the centre (cf. figure 2*c*). (*b*) Outer source jets on the sidewalls are closer to the corners (cf. figure 2*f*).

points of the sidewalls, a large fluctuating central vortex results (figure 3*b*). In this case, the sources near the corners merge and act like corner sources directed toward the centre, hence making the configuration similar to figure 2(*b*) of eight-pair forcing.

We use the configurations in figure 2 and denote those leading to the single-vortex pattern as S-configurations (figure 2*a–c*) and those leading to an unsteady irregular state as I-configurations (figure 2*d–f*).

3. Results

3.1. *Temporal variation*

Figure 4 shows the velocity and streamfunction field of the twelve-pair S-configuration (figure 2*c*) in a two-layer stratification. Strong single-vortex patterns appear intermittently. We note that out of five observed appearances, the single vortex is clockwise in four (2–6 h, 10–14 h, 38 h, 50–58 h) and counterclockwise in one (28 h). Similar behaviours are observed with other S-configurations.

Temporal variations of the spatially averaged velocity magnitude are shown in figure 5 for the six configurations of figure 2. The filled circles denote strong single vortices, the triangles weak or deformed single vortices, and the crosses irregular states. The sign of the vorticity is indicated above the filled circles. Two squares in figure 5(*d*) (four-pair I-configuration) represent a strong dipolar velocity field observed only for this configuration. The single-vortex pattern appears with all the configurations, but the velocity magnitude is distinctly larger for the S-configurations (figure 5*a–c*) than for the I-configurations (figure 5*d–f*). Particularly, with the eight-pair I-configuration, the single-vortex pattern appears as frequently as with the S-configuration, but the

https://doi.org/10.1017/S0022112002008182 Published online by Cambridge University Press

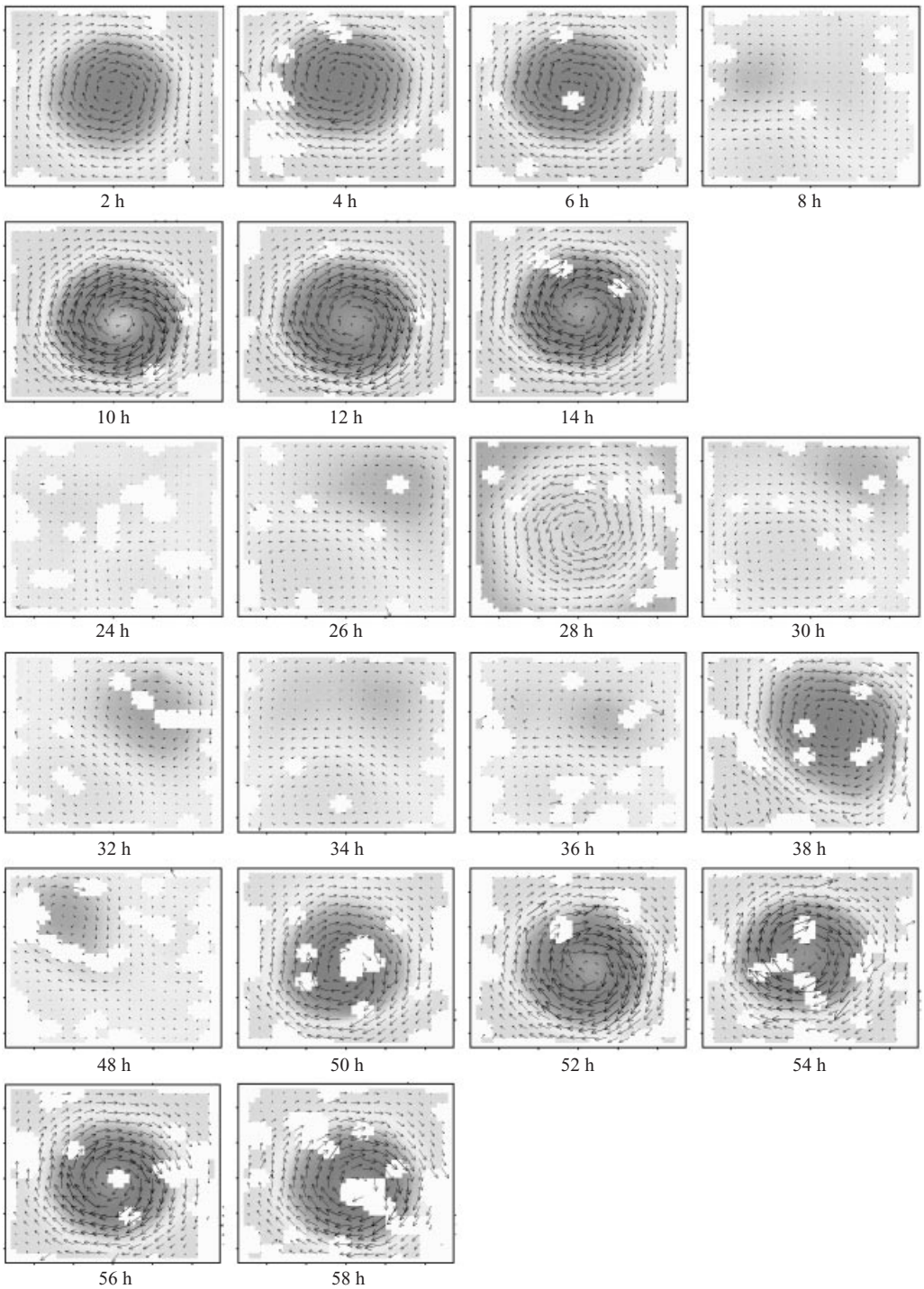


FIGURE 4. Velocity and streamfunction fields at the density step forced by the twelve-pair S-configuration in the kerosine–salt water experiments. Unfilled cells are caused by shortage of tracked particles. The darkness of the streamfuction field is not proportional to the amplitude.

https://doi.org/10.1017/S0022112002008182 Published online by Cambridge University Press

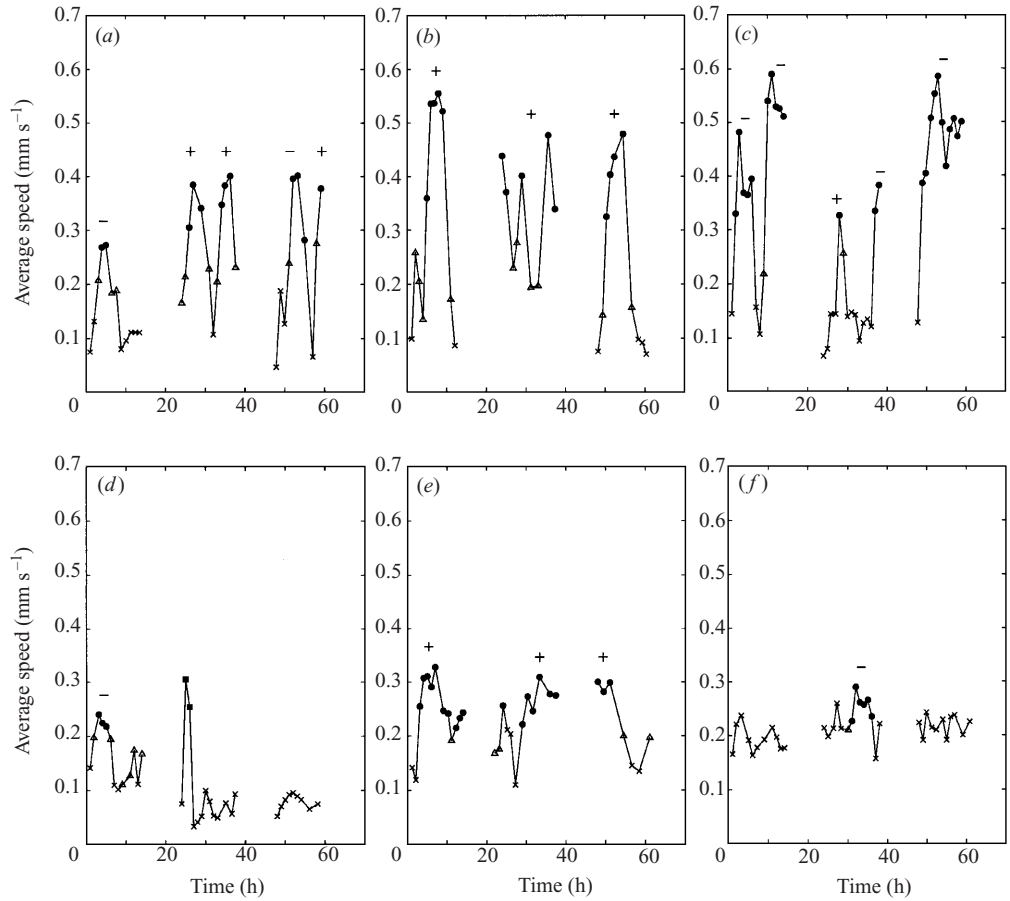


FIGURE 5. Temporal variation of spatially averaged velocity magnitude at the density step in the kerosine–salt water experiments. The forcing configurations for (*a–f*) are given in figure 2. Filled circle: clear single-vortex pattern, triangle: deformed unclear single-vortex pattern, cross: irregular pattern, filled square: dipolar pattern. The signs above the filled circles represent the signs of the vorticity.

kinetic energy attained is much smaller than with the S-configuration. Hence the behaviour in a linear stratification is reflected in the behaviour at the interface in a two-layer stratification even though the source jets are supposed to interact three-dimensionally in the homogeneous lower layer. Also we note that the variation period of the velocity magnitude is approximately the same (5–10 h) for all the configurations. This indicates that the time scale of variation of the large-scale flow structure due to jet interaction is not sensitive to the forcing configuration, and the distinctly large velocity magnitudes are related to a flow field that can be achieved only by the S-configurations. We next examine how 'three-dimensionally' the source jets are interacting in the lower layer and identify the flow field related to the large velocity magnitudes.

3.2. *Vertical structure*

We visualize the velocity field in the forcing plane. For this purpose, the kerosine–salt water combination is not suitable because Pliolite particles are trapped at the interface

https://doi.org/10.1017/S0022112002008182 Published online by Cambridge University Press

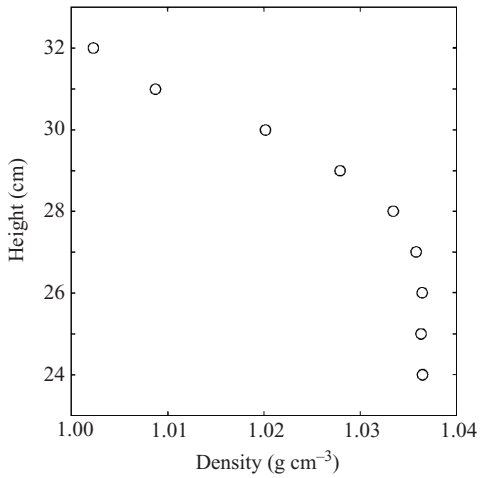


FIGURE 6. Vertical density profile for a fresh–salt water experiment with $H = 30$ cm. The measurement was taken 24 h after filling the tank.

and react with kerosine even if their density is larger than that of the salt water. To resolve this problem, fresh water is used instead of kerosine. The depth H of the lower salt water (density $\sim 1.036\,\mathrm{g\,cm^{-3}}$) is 10, 20, and 30 cm. Fresh water is added slowly through sponge foam to minimize mixing with the salt water. A 3 cm-thick layer is formed. The density profile for $H = 30$ cm after 24 h of interface formation is shown in figure 6. Pliolite VT particles are seeded at the interface ($z = 29$ cm for $H = 30$ cm). The buoyancy frequency at the seeded plane is initially about $3.6\,\mathrm{s^{-1}}$ and decreases to about $2.7\,\mathrm{s^{-1}}$ in 20 h. With this stratification, the four- and eight-pair S-configurations are tested.

The results are shown in table 1 by qualitative classification from A to D. The state A has similar appearance to the single-vortex pattern in a linear stratification, i.e. the single-vortex pattern is maintained during the run. The state B behaves similarly to the intermittent strong single-vortex pattern in the kerosine–salt water experiments. The state C has a weak single-vortex pattern similar to the eight-pair I-configuration in the kerosine–salt water experiments. The state D is unsteady and irregular. Although we always obtain state B for the S-configurations with the kerosine–salt water experiments, the probability here of obtaining state B is much smaller for $H = 20, 30$ cm. It suggests that a large density gradient is necessary to obtain state B. State A for $H = 10$ cm is due to the sufficiently large density gradient at the forcing height. As we can see in figure 6, a non-negligible density gradient exists 4 cm below the seeded plane and the forcing jets 5 cm below the seeded plane result in a velocity field similar to that in a linear stratification. During each run, molecular diffusion of salt spreads the density profile by about 1 cm and the forcing jets for $H = 20, 30$ cm are not directly affected by the stratification. Indeed there was no noticeable temporal increase in the frequency of appearance of the single-vortex pattern for $H = 20, 30$ cm.

The horizontal velocity field below the interface is observed by sprinkling Pliolite AC particles (density $\sim 1.042\,\mathrm{g\,cm^{-3}}$) on the surface. The particles fall through the lower layer at about $0.8\,\mathrm{mm\,s^{-1}}$. Horizontal slit lights of 2 cm thickness are used and the streak images of the horizontal motion are recorded while the particles fall through the illuminated layer.

https://doi.org/10.1017/S0022112002008182 Published online by Cambridge University Press

Configuration	H (cm)	Run	Duration	Result	Comment
4S	10	00MC111	16 h	A	
		00MC221	20 h 45 m	A	
		00MC291	20 h	A	
	20	00MC191	15 h	B	
		00MC251	23 h 30 m	D	
		00MY041	20 h 40 m	B	b
	30	00MC151	20 h 30 m	B	b
		00MC171	21 h	C	
		00MC271	32 h 45 m	D	
8S	10	00AP121	9 h	A	
		00AP131	9 h	A	
		00AP132	9 h	A	
	20	00AP141	19 h 25 m	B	b
		00AP271	19 h	C	
		00AP281	25 h 10 m	C	
	30	00AP041	18 h	D	
		00AP051	18 h	C	b
		00AP061	23 h	D	
		00AP081	19 h	D	
		00AP101	17 h	B	b

TABLE 1. List of the fresh–salt water experiments. The results are classified as A: persistent single-vortex pattern, B: intermittent strong single-vortex pattern, C: intermittent weak single-vortex pattern, D: unsteady and irregular. Vertical structures are observed in figures 7 and 8 for the runs marked 'b'.

Horizontal streak images are taken at various heights for the runs marked 'b' in table 1. The results are shown in figures 7 and 8 for $H = 20$ and 30 cm, respectively. For nearly steady states (those except for figure 8*b*), the velocity field at the density interface is calculated by DigImage to compare the velocity magnitudes. The circulation in $\mathrm{mm^2\,s^{-1}}$ along a circle of radius 150 mm with the origin at the centre of the vortex is shown below the velocity field. The centre of the vortex is determined at the location of the minimum velocity magnitude. When there is a strong single vortex at the interface (figure 7*a*; figure 8*a*, *d*), the single-vortex structure extends down to the forcing height. In other cases (figure 7*b*, *c*; figure 8*b*, *c*, *e*), the streak images in the forcing plane are irregular.

Our interpretation is as follows. The source jets are principally horizontal, but since they interact three-dimensionally, the resulting velocity field in the lower layer is unsteady and irregular. However, near the orifices of the forcing pipes, the source jets are unaffected by the other source jets and the horizontal velocity components are diffused onto the density interface. If the forcing configuration is S-type, there are centrally directed steady components at the density interface. With such velocity components, there is a high probability that the interfacial flow becomes similar to the single-vortex pattern produced by jets deflecting each other. At this stage, the single-vortex pattern may be disturbed by the irregular flow in the interior. However, if the velocity field happens to have the property of an eigenmode of the Helmholtz equation, i.e. the vorticity is proportional to the streamfunction and the proportionality constant is equal to the corresponding eigenvalue, then the velocity can attain large magnitude by resonance. The strong horizontal flow at the interface then makes the flow in the lower layer nearly horizontal by viscous friction. The S-configuration

https://doi.org/10.1017/S0022112002008182 Published online by Cambridge University Press

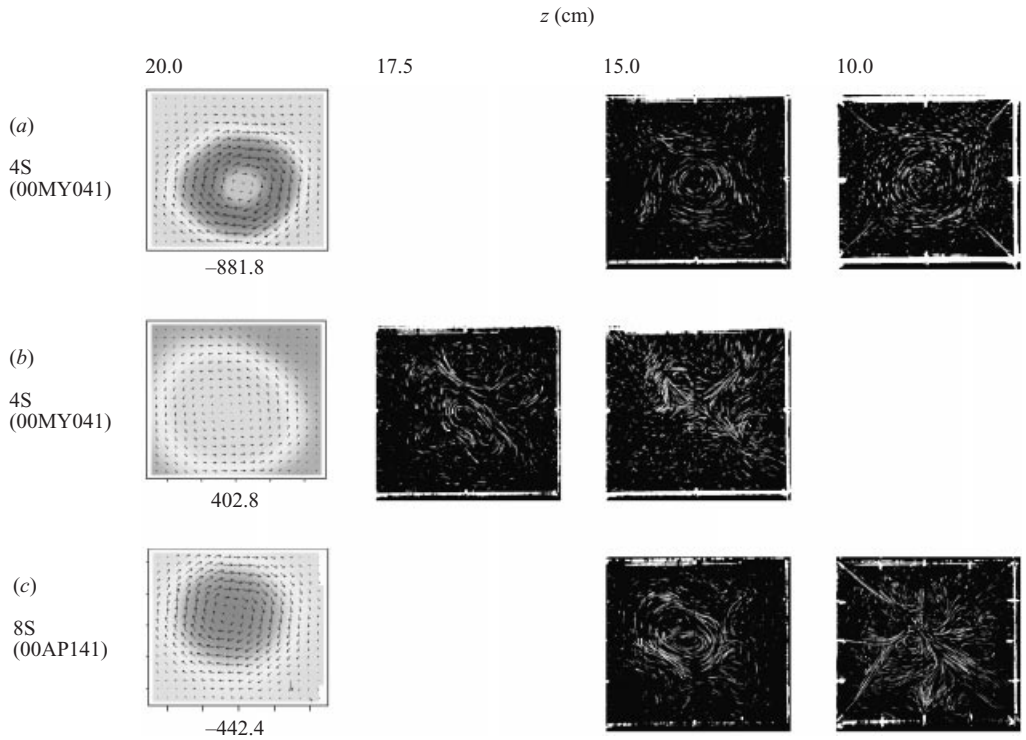


FIGURE 7. Horizontal fields at various heights for the fresh–salt water experiments with $H = 20$ cm. The particle-tracked velocity fields are shown at the largest density gradient. The numbers beneath the velocity fields are the circulation in $\mathrm{mm^2\,s^{-1}}$ along a circle of radius 150 mm with the origin at the centre of the vortex.

results in the single-vortex pattern in the forcing plane and kinetic energy is efficiently supplied to the interfacial flow. Vertical coherence is thus established. Although we described the evolution as a two-step process of eigenmode formation at the interface and redirection into the horizontal in the forcing plane, they are expected to occur concurrently. Due to the resonant amplification, the single-vortex structure is stable to disturbances and remains for hours until a sufficiently large disturbance destroys it. The dipolar pattern observed with the four-pair I-configuration is also an eigenmode for the square domain. With the I-configurations, the disturbances at the forcing plane are large and the resonant state which must be quasi-two-dimensional cannot be established.

3.3. *ψ–ω relation*

In this subsection, we verify that the single-vortex pattern has the property of the lowest eigenmode. First, we recapitulate the argument of KL.

When the flow is steady and vertical coherence is established, vertical shear becomes negligible compared to horizontal shear and the flow is approximately two-dimensional. With length scale 200 mm and velocity scale $2\,\mathrm{mm\,s^{-1}}$ (typical values for the single-vortex pattern), the Reynolds number is 40. Hence at the leading order, the steady-state vorticity equation is reduced to

$$J(\nabla^2\psi, \psi) = 0, \tag{3.1}$$

where ψ is the streamfunction and J is the Jacobian. The general solution to (3.1) is

https://doi.org/10.1017/S0022112002008182 Published online by Cambridge University Press

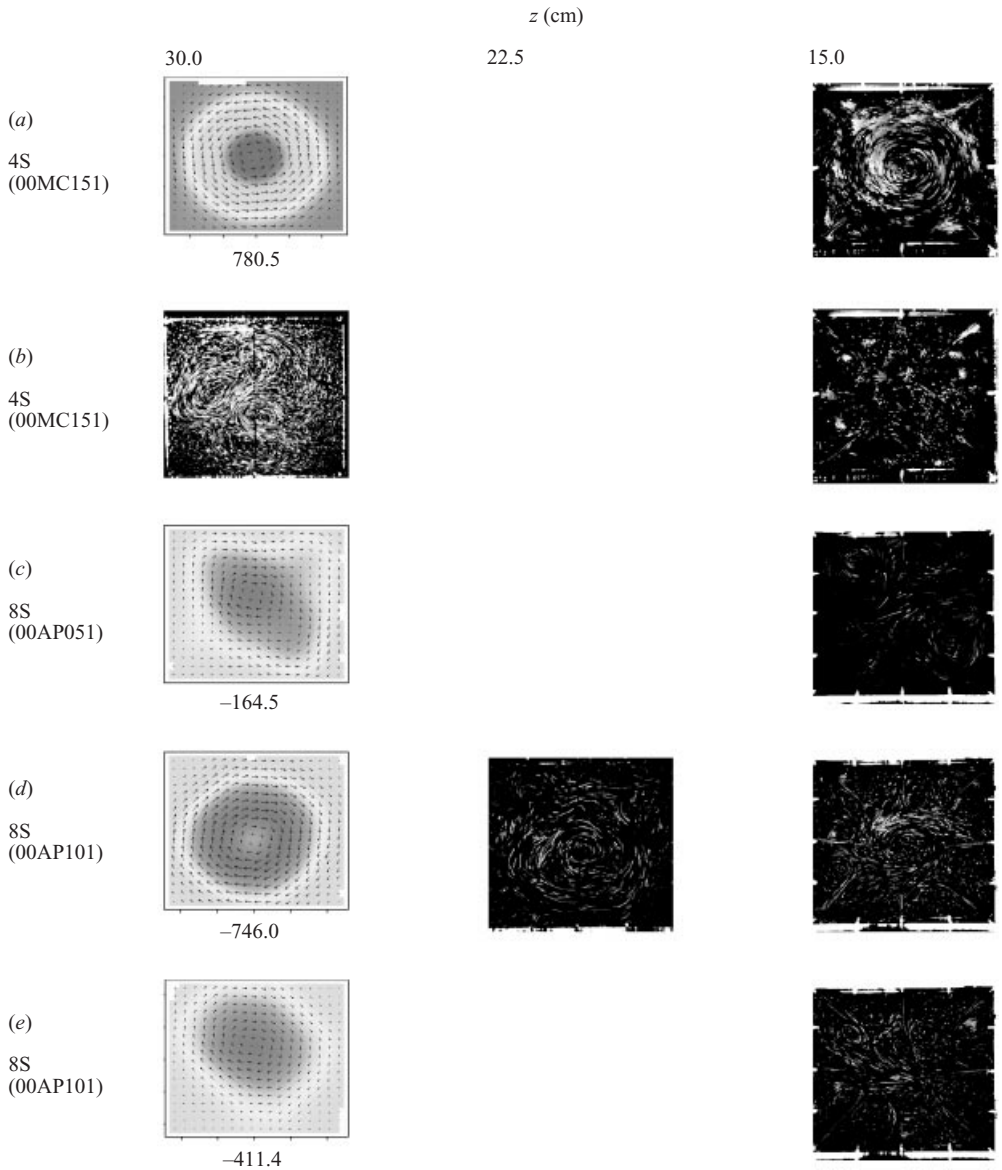


FIGURE 8. As figure 7 but with $H = 30\,\text{cm}$. The particle-tracked velocity fields are shown at the largest density gradient except for 00MC151 which is unsteady and irregular.

given by $\nabla^2\psi = f(\psi)$, where f is an arbitrary continuously differentiable function of ψ. Assuming a linear functionality $f(\psi) = -\lambda^2\psi$, we obtain the Helmholtz equation

$$\nabla^2\psi = -\lambda^2\psi. \tag{3.2}$$

The boundary condition for this equation is the source–sink forcing on the sidewalls. Although the forcing is arranged in configurations which do not impart net angular momentum or thrust, experimental errors always exist. We decompose the solution into three parts $\psi = \psi_0 + \psi_1 + \psi_2$, where $\nabla^2\psi_i = -\lambda^2\psi_i$ $(i = 0, 1, 2)$, and ψ_0 satisfies the boundary condition without net angular momentum or thrust, ψ_1 satisfies the

https://doi.org/10.1017/S0022112002008182 Published online by Cambridge University Press

boundary condition corresponding to the experimental errors, and ψ_2 satisfies the homogeneous boundary condition ($\psi_2 = 0$) on the sidewalls. Only when λ^2 is equal to one of a set of discreet values (eigenvalues), is the last part ψ_2 non-zero and is called an eigenmode. The amplitude of ψ_2 is arbitrary. When λ^2 is not an eigenvalue, ψ_0 and ψ_1 have finite amplitudes proportional to their amplitudes on the boundary. However, when λ^2 approaches certain eigenvalues, the amplitude of ψ_0 remains finite while the amplitude of ψ_1 tends to infinity. The form of ψ_1 becomes approximately the same as the corresponding eigenmode. Such a resonant amplification of an eigenmode is a general property of the Helmholtz equation, and detailed algebra specific to the source–sink forcing experiments appears in Kanda (2001). This eigenmode resonance occurs at the lowest eigenvalue in a square domain and induces significantly larger circulation than can be achieved without resonance. The single-vortex patterns in figure 2 correspond to the lowest eigenmode $\psi \sim \cos(\pi x/L)\cos(\pi y/L)$ with $\lambda^2 = 2\pi^2/L^2$, where the square domain is defined by $-1/2 \leqslant x/L \leqslant 1/2$, $-1/2 \leqslant y/L \leqslant 1/2$ and L is the length of a side. The choice of the linear function $f(\psi) = -\lambda^2\psi$ is not justified in mechanical terms, but such a resonant behaviour is known only for the Helmholtz equation. We emphasize that the eigenmode argument is introduced to explain the steady states with significant circulation, and does not apply to unsteady states.

The distinctly large velocity magnitudes in the form of the single-vortex pattern in figure 5(*a–c*) are considered to be caused by this resonance mechanism. We examine the relation between the stream function ψ and the vorticity, $\omega = -\nabla^2\psi$ to see whether the observed single-vortex patterns have the property of the Helmholtz equation. In the linear stratification experiments, the domain boundary is the sidewalls where the forcing exists, but in the kerosine–salt water experiments, the forcing is well inside the sidewalls because it acts through viscous diffusion from below the density interface. Considering a square domain with free-slip boundary condition on the sidewalls and forcing in the interior is mathematically intractable. Instead of developing a theory applicable to general steady states, we consider a simplified model specific to the single-vortex pattern. In the single-vortex pattern, the fluid is trapped inside the central vortex, exchanging with the exterior only at the locations where the source jets merge with the central vortex. Hence we consider a circular domain of a diameter $2R$ with forcing at the perimeter. Any polygon reflecting the number of sources may be used, but since we will need the approximate magnitude of the eigenvalue of the lowest eigenmode and it is determined by the representative size of the domain, we choose a circle for simplicity. The lowest eigenmode is then $\psi \sim J_0(\lambda r)$ with the eigenvalue $\lambda^2 = (v_0/R)^2$, where J_0 is the zeroth-order Bessel function, r is the radial coordinate, and v_0 is the smallest root of $J_0(x) = 0$.

The relation between the vorticity ω and the streamfunction ψ is shown in figure 9 for representative single-vortex patterns (filled circles in figure 5) corresponding to the forcing configurations in figure 2(*a–f*). The corresponding velocity fields look similar to the single-vortex patterns in figure 4 for all the configurations. The streamfunction ψ is calculated such that the average of ψ over the analysed region is zero. While the four-pair S-configuration (figure 9*a*) and I-configurations (figure 9*d–f*) have approximately linear relations over the whole domain, the eight- and twelve-pair S-configurations (figure 9*b*, *c*) have two linear segments with different slopes. When the flow is unidirectional in azimuth as in the single-vortex pattern, the streamfunction changes monotonically with respect to the radius (figure 10). We regard the larger $|\psi|$ segments, which correspond to the central region in the flow domain, as belonging to the resonant eigenmode. The smaller $|\psi|$ segments correspond to the region near the

https://doi.org/10.1017/S0022112002008182 Published online by Cambridge University Press

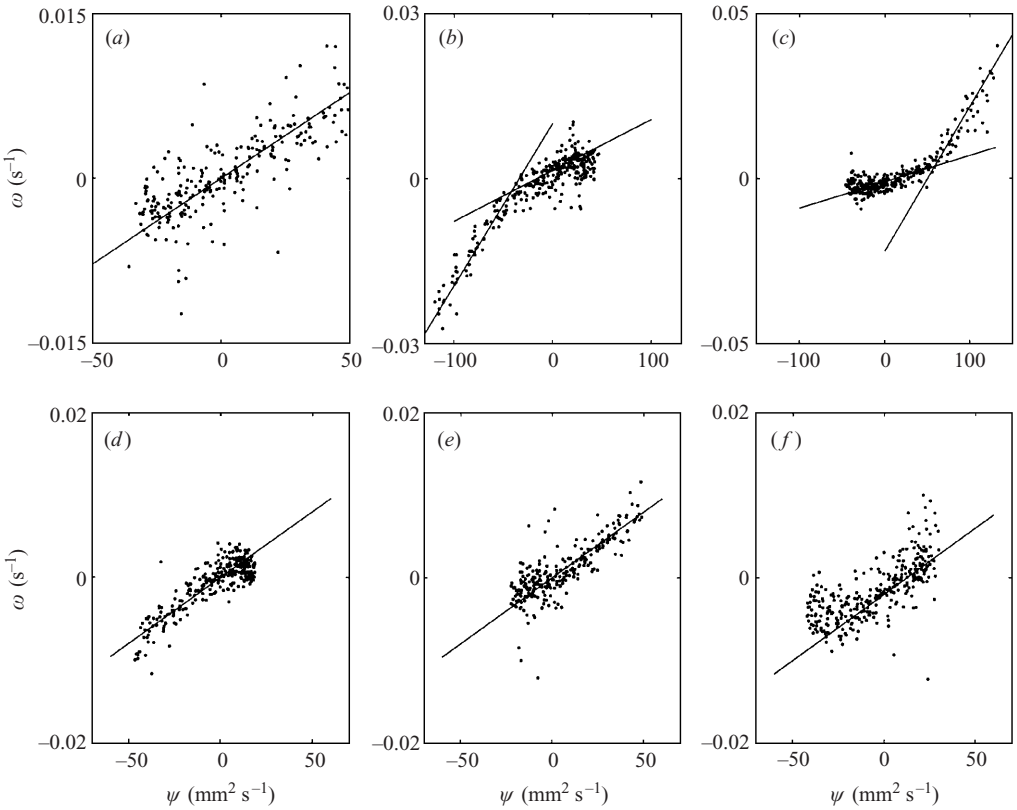


FIGURE 9. Relation between the streamfunction ψ and the vorticity ω for the kerosine–salt water experiments. The forcing configurations are the same as figure 2(*a–f*). The data are for the single-vortex patterns (filled circles in figure 5). The lines in (*a*, *d–f*) have the same slope corresponding to $2R = 385$ mm.

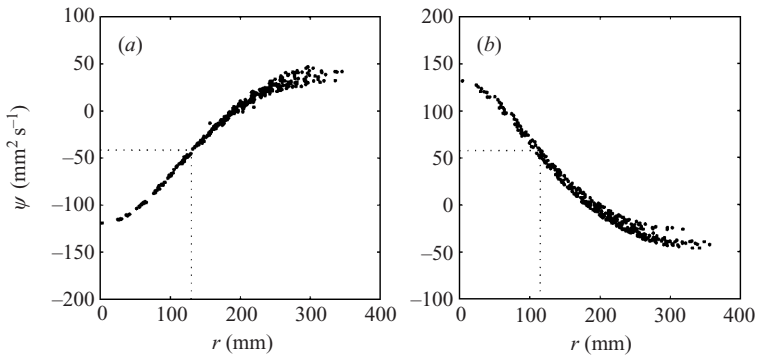


FIGURE 10. Relation between the radius r from the vortex centre and the streamfunction ψ: (*a*) eight-pair S-configuration (figure 9*b*), (*b*) twelve-pair S-configuration (figure 9*c*). The dotted lines indicate the radii corresponding to the values of ψ at the crossing points of the lines in figure 9.

sidewalls outside the single vortex. The radii corresponding to the dividing values of ψ are 130 and 115 mm for figures 9(*b*) and 9(*c*), respectively. As shown in figure 2(*a–c*), the region outside the central vortex is much smaller for the four-pair S-configuration than for the eight- and twelve-pair S-configurations, and this is why there is only one

https://doi.org/10.1017/S0022112002008182 Published online by Cambridge University Press

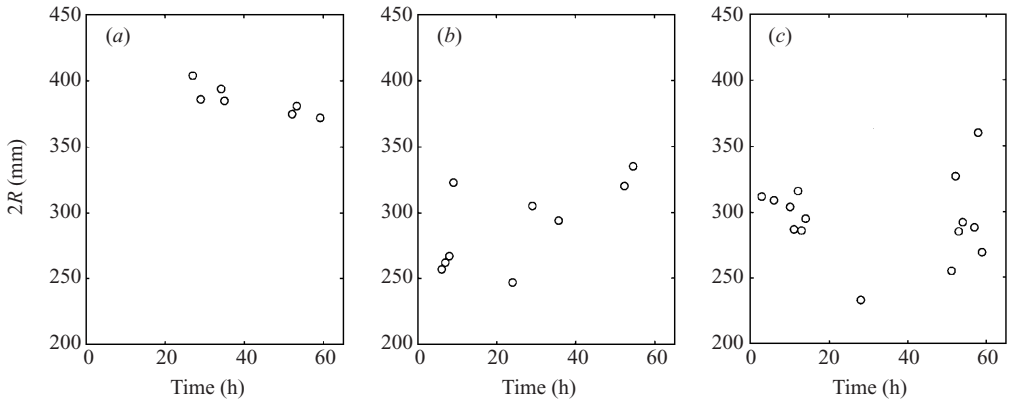


FIGURE 11. Diameter $2R$ of the effective domain for the single-vortex patterns. The values are calculated only for the single-vortex patterns. The forcing configurations are the same as figure 2(a–c).

linear segment in figure 9(a). When a strong single vortex is observed at the interface, the effective domain diameter $2R$ is calculated from the slope of the ψ–ω relation (figure 11). The obtained diameters are comparable to those of the observed vortices in a linear stratification (figure 2a–c). The value of $2R$ is larger for the four-pair S-configuration than for the eight- and twelve-pair S-configurations. It is consistent with the size of the single vortices in a linear stratification of figure 2. Also, although a little larger, the radii R obtained from the slopes of the ψ–ω relation are comparable to the radii corresponding to the dividing values of ψ in figures 9(b) and 9(c). The single-vortex patterns of the I-configurations have slopes approximately equal to that of the four-pair S-configuration. The slope of the lines on figure 9 corresponds to $2R = 385$ mm. We note that a single-vortex pattern without coupling with the forcing plane has about this size, and do not further examine this coincidence.

4. Discussion

First, we summarize the results, and then discuss three aspects: energy balance of the eigenmode state, relevance to two-dimensional turbulence, and practical applications.

We studied the velocity field at the density interface of a two-layer stratification system when the flow is forced at the mid-depth of the lower layer by the source–sink forcing method. Two types of forcing configuration are used: one that leads to a steady single-vortex pattern in a linear stratification, and the other that results in an unsteady irregular state. Strong single-vortex patterns appear intermittently for the former configurations. They are identified as the lowest eigenmode of the Helmholtz equation for the streamfunction. Resonant amplification of the eigenmode and the tendency of the forcing configuration to produce the single-vortex pattern cooperate to stabilize a vertically coherent single-vortex structure. While KL shows the evidence of three different eigenmode structures in a linear stratification, this paper shows that the linear stratification is not necessary to obtain the lowest eigenmode structure and reveals the resonating behaviour as energy accumulation into the lowest eigenmode.

We discuss the amplitude of an eigenmode in terms of energy balance. With a fixed amount of energy supply from the forcing, an unsteady irregular state, whether quasi-horizontal or fully three-dimensional, establishes energy balance by viscous dissipation in the relatively small-scale shear field. For a quasi-two-dimensional steady state with

https://doi.org/10.1017/S0022112002008182 Published online by Cambridge University Press

moderate horizontal velocity, dissipation due to vertical shear is smaller than in the unsteady states because the horizontal velocity decreases monotonically from the forcing height to zero at the bottom of the tank. To achieve energy balance, the velocity magnitude at the forcing height must become large. The Helmholtz equation provides a mechanism to accumulate kinetic energy in the form of an eigenmode. A non-resonant quasi-horizontal flow cannot attain sufficiently large velocity magnitude and becomes unsteady in order to increase vertical shear. The velocity magnitude of the eigenmode state can be estimated by this energy argument. In the source–sink forcing experiments, the energy input for n source–sink pairs with the forcing velocity V is proportional to nV^2. If the representative horizontal velocity magnitude is U, viscous dissipation is proportional to U^2. When the horizontal flow is almost circular and viscous diffusion reduces the horizontal shear, viscous dissipation is mostly due to the vertical shear. The energy balance requires $U \propto \sqrt{n}V$. The same relation is observed by de Rooij, Linden & Dalziel (1999) from similar source–sink experiments in a circular domain. In our experiments, approximate proportionality to $\sqrt{n}$ is seen in figure 5(a–c): the peak average speed is 0.4, 0.55, 0.6 mm s^{-1} for $n = 4, 8, 12$, respectively. The relatively small speed for $n = 12$ is probably because not all the twelve source jets are contributing to the central vortex as can be seen in figure 2(c).

The organizing behaviour of the source–sink forced flows resembles that of forced two-dimensional turbulence in a bounded domain. Here we discuss the difference. First, we briefly review related work. For two-dimensional turbulence, Kraichnan (1967) predicts energy transfer from the forcing scale to larger scales and accumulation of energy in the largest structure the flow domain can accommodate. Paret & Tabeling (1998), in their laboratory experiments, use electromagnetic forcing in a thin layer of salt water to create irregular quasi-two-dimensional flows, and observe a dominant vortex when the effect of bottom friction is small. Numerical experiments show similar organizing behaviour, but they are unforced unbounded (Bracco *et al.* 2000; Dritschel 1993), forced unbounded (Smith & Yakhot 1994; Legras, Santangelo & Benzi 1998), or unforced bounded (Li & Montgomery 1996; Clercx, Maassen & van Heijst 1999). The source–sink forced flows are distinctly different from two-dimensional turbulence in that the turbulence is controlled by the forcing on the sidewalls. A fundamental assumption of two-dimensional turbulence is that the velocity field is homogeneous, at least locally, and the properties of the flow are independent of the nature of the forcing. The forcing of Paret & Tabeling (1998) is uniformly distributed in the domain and simulates two-dimensional turbulence properly. In contrast, the source jets in the source–sink forcing experiments decay by viscous friction as they advance horizontally into the domain, and the supply of kinetic energy is not uniform in the domain. As shown in figure 2, the induced flows exhibit sensitivity to the forcing configuration, which is expected of two-dimensional turbulence. As emphasized in KL, the organizing behaviour in a linear stratification should be studied in terms of laminar jet interaction. Laminar jet interaction, however, is known to show highly complicated bifurcation behaviour (e.g. Goodwin & Schowalter 1996). The eigenmode resonance argument does not relate the individual forcing configurations to the resultant flows, but it is useful in explaining the emergence of steady states with significant circulation. We also note that the linear relationship between the streamfunction and vorticity of an eigenmode state (figure 9) should not be confused with the linear relationships of the maximum-entropy state (Chavanis & Sommeria 1996) or minimum-enstrophy state (Leith 1984). The maximum-entropy state is a macroscopic realization of a purely inviscid two-dimensional turbulence and the minimum-enstrophy state is a hypothesized long-time limit of a decaying viscous two-dimensional turbulence.

https://doi.org/10.1017/S0022112002008182 Published online by Cambridge University Press

Our work is motivated by scientific interest and does not address specific practical problems, but we point out some possible directions. Firstly, our results are limited to bounded flows because eigenmode resonance requires a finite domain. Fluctuating leaks of net angular momentum or thrust by the flow across the domain boundary would not satisfy the condition for the eigenmode resonance. The boundary walls also help establish the single-vortex pattern by attracting the jets to the walls through the Coanda effect. Secondly, our results are not necessarily limited to laminar flows. As discussed in Voropayev & Afanasyev (1994), if we are, for example, concerned with the interaction of large-scale structures in an ocean basin, the effective Reynolds number is moderate because the large-scale structures evolve against the background of small-scale motions which provide an eddy viscosity much larger than the molecular viscosity of salt water. This picture is justified by the observations of the gap in the energy spectrum between the large-scale structures and the small-scale motions in the ocean. Thirdly, the two-layer stratification has analogues in the thermocline of the ocean or the upper troposphere in the atmosphere, where the flow forcing is usually separated from the steepest density gradient. Particularly, the single-vortex pattern resembles the antarctic polar vortex which exhibits an annual cycle between quasi-steady and irregular states although the generation mechanisms are different and Earth's rotation plays an important role. The polar vortex contains low-ozone air and the horizontal mixing at the perimeter is an important environmental issue. While mixing in an irregular state is obvious, mixing in a quasi-steady state occurs through folding and stretching by Rossby wave-breaking at the vortex boundary (e.g. Bowman & Magnus 1993). Such Lagrangian mixing or chaotic advection occurs in our experiments through the fluctuating velocity field outside the central vortex.

We have shown that the formation of the single-vortex pattern depends on the forcing configuration, but have not yet given a satisfactory explanation for why some configurations result in the single-vortex pattern and others do not. Our empirical rule is that the single-vortex pattern appears when all the source jets are directed toward the centre of the domain. We are currently working with rectangular and triangular domains to confirm this rule.

I.K. is supported by the Blasker Fellowship.

REFERENCES

Boubnov, B. M., Dalziel, S. B. & Linden, P. F. 1994 Source-sink turbulence in a stratified fluid. *J. Fluid Mech.* **261**, 273–303.

Bowman, K. P. & Magnus, N. J. 1993 Observations of deformation and mixing of the total ozone field in the antarctic polar vortex. *J. Atmos. Sci.* **50**, 2915–2921.

Bracco, A., McWilliams, J. C., Murante, G., Provenzale, A. & Weiss, J. B. 2000 Revisiting freely decaying two-dimensional turbulence at millennial resolution. *Phys. Fluids* **12**, 2931–2941.

Chavanis, P. H. & Sommeria, J. 1996 Classification of self-organized vortices in two-dimensional turbulence: the case of a bounded domain. *J. Fluid Mech.* **314**, 267–297.

Clercx, H. J. H., Maassen, S. R. & van Heijst, G. J. F. 1999 Decaying two-dimensional turbulence in square containers with no-slip or stress-free boundaries. *Phys. Fluids* **11**, 611–626.

Dalziel, S. B. 1993 Rayleigh–Taylor instability: experiments with image analysis. *Dyn. Atmos. Oceans* **20**, 127–153.

Dritschel, D. G. 1993 Vortex properties of two-dimensional turbulence. *Phys. Fluids* A **5**, 984–997.

Goodwin, R. T. & Schowalter, W. R. 1996 Interactions of two jets in a channel: solution multiplicity and linear stability. *J. Fluid Mech.* **313**, 55–82.

Kanda, I. 2001 Interaction of quasi-horizontal jets in bounded domains. PhD thesis, University of California, San Diego.

https://doi.org/10.1017/S0022112002008182 Published online by Cambridge University Press

KANDA, I. & LINDEN, P. F. 2001 Sensitivity of horizontal flows to forcing geometry. *J. Fluid Mech.* **432**, 419–441 (referred to herein as KL).

KRAICHNAN, R. H. 1967 Inertial ranges in two-dimensional turbulence. *Phys. Fluids* **10**, 1417–1423.

LEGRAS, B., SANTANGELO, P. & BENZI, R. 1988 High-resolution numerical experiments for forced two-dimensional turbulence. *Europhys. Lett.* **5**, 37–42.

LEITH, C. E. 1984 Minimum enstrophy vortices. *Phys. Fluids* **27**, 1388–1395.

LI, S. & MONTGOMERY, D. 1996 Decaying two-dimensional turbulence with rigid walls. *Phys. Lett.* **218**, 281.

LINDEN, P. F., BOUBNOV, B. M. & DALZIEL, S. B. 1995 Source-sink turbulence in a rotating stratified fluid. *J. Fluid Mech.* **298**, 81–112.

PARET, J. & TABELING, P. 1998 Intermittency in the two-dimensional inverse cascade of energy: Experimental observations. *Phys. Fluids* **10**, 3126–3136.

DE ROOIJ, F., LINDEN, P. F. & DALZIEL, S. B. 1999 Experimental investigations of quasi-two-dimensional vortices in a stratified fluid with source-sink forcing. *J. Fluid Mech.* **383**, 249–283.

SMITH, L. M. & YAKHOT, V. 1994 Finite-size effects in forced two-dimensional turbulence. *J. Fluid Mech.* **274**, 115–138.

VOROPAYEV, S. I. & AFANASYEV, Y. D. 1994 *Vortex Structures in a Stratified Fluid*. Chapman & Hall.

https://doi.org/10.1017/S0022112002008182 Published online by Cambridge University Press